Lithium Metal Batteries

How to cite:
International Edition: doi.org/10.1002/anie.202101627
German Edition: doi.org/10.1002/ange.202101627

Non-Solvating and Low-Dielectricity Cosolvent for Anion-Derived Solid Electrolyte Interphases in Lithium Metal Batteries

*Jun-Fan Ding[+], Rui Xu[+], Nan Yao[+], Xiang Chen, Ye Xiao, Yu-Xing Yao, Chong Yan, Jin Xie, and Jia-Qi Huang**

Abstract: *Lithium (Li) metal anodes hold great promise for next-generation high-energy-density batteries, while the insufficient fundamental understanding of the complex solid electrolyte interphase (SEI) is the major obstacle for the full demonstration of their potential in working batteries. The characteristics of SEI highly depend on the inner solvation structure of lithium ions (Li^+). Herein, we clarify the critical significance of cosolvent properties on both Li^+ solvation structure and the SEI formation on working Li metal anodes. Non-solvating and low-dielectricity (NL) cosolvents intrinsically enhance the interaction between anion and Li^+ by affording a low dielectric environment. The abundant positively charged anion–cation aggregates generated as the introduction of NL cosolvents are preferentially brought to the negatively charged Li anode surface, inducing an anion-derived inorganic-rich SEI. A solvent diagram is further built to illustrate that a solvent with both proper relative binding energy toward Li^+ and dielectric constant is suitable as NL cosolvent.*

Introduction

With the ever-increasing global energy demands for portable electronic devices, electric vehicles, and large-scale grids, lithium (Li) metal with an extremely high theoretical specific capacity (3860 $mAh\,g^{-1}$) and most negative electrochemical potential (−3.040 V vs. the standard hydrogen electrode) has attracted intensive attention as one of the most promising anode materials to power next-generation high-energy-density rechargeable batteries.[1] However, the poor reversibility and inferior safety originated from the dendritic Li growth intensely impede the practical applications of Li metal anodes.[2,3]

Due to the ultra-high reactivity of lithium metal, the inevitable reactions between conventional electrolytes and lithium induce the instantaneous generation of an ionically conductive but electronically insulative solid electrolyte interphase (SEI).[4] The heterogeneity and fragility of SEI are commonly considered as the major origins of the severe dendritic Li growth.[2,5] Hence, the rational regulation of a chemically homogeneous and mechanically robust SEI is the primary pre-request to enable high-efficiency and long-lifespan working Li metal batteries.[6]

The inner solvation structure of Li ion (Li^+) plays an essential role in determining the SEI characteristics.[7,8] Two major strategies have been reported to regulate the primary Li^+ solvation shell. The first strategy is the regulation of electrolyte compositions by intuitively tunning the Li^+ solvation structure by solvents with a high Gutmann donor number (DN). The components featuring with higher DN are more favorably to be recruited into the inner solvation shell.[9] Additionally, Li^+ solvation behavior can be readily manipulated through increasing the salt concentration. A higher concentration favors more anion participation into solvation shells around Li^+ since the deficiency of available solvents.[10] A novel concept of localized high-concentration electrolyte (LHCE) has been widespread recently to further reduce the viscosity of high-concentration electrolyte (HCE) by introducing "inert" fluorinated ether cosolvent, where the original solvation units are believed to be "maintained".[11] Despite the prominent performance, the fundamental physicochemical understanding behind the electrolyte with the presence of so-called "inert" cosolvent is less explored.

In this contribution, we described a general principle that a type of non-solvating and low-dielectricity (NL) cosolvent can intrinsically facilitate the anion-cation interaction, and thus promote the generation of aggregates (AGGs, an anion coordinating to two or more Li^+) via model investigations. Generally, cosolvents with weak binding strength with Li^+ and low permittivity considerably enhance the interaction between anions and Li cations by affording a specific low-dielectricity environment. The domination of positively charged AGG structures in electrolytes enables the substantial accumulation of anions at the negatively charged Li surface, which accelerates the anion decomposition to form an anion-derived inorganic-rich SEI. A solvent diagram was further built based on the descriptors of relative binding energy towards Li^+ and dielectric constant to explicitly identify the criteria of a suitable NL cosolvent.

[*] J.-F. Ding,[+] R. Xu,[+] Y. Xiao, Dr. C. Yan, Prof. J.-Q. Huang
School of Materials Science and Engineering, Beijing Institute of Technology
Beijing 100081 (P. R. China)
and
Advanced Research Institute of Multidisciplinary Science, Beijing Institute of Technology
Beijing 100081 (P. R. China)
E-mail: jqhuang@bit.edu.cn
N. Yao,[+] Dr. X. Chen, Y.-X. Yao, Dr. C. Yan, J. Xie
Department of Chemical Engineering, Tsinghua University
Beijing 100084 (China)
[+] These authors contributed equally to this work.
Supporting information and the ORCID identification number(s) for the author(s) of this article can be found under: https://doi.org/10.1002/anie.202101627.

Results and Discussion

The model electrolytes employed in this work consist of simplified ether electrolyte, 3.0 mol L^{-1} (M) LiFSI/DME, with or without NL cosolvent. 1,1,2,2-Tetrafluoroethyl 2,2,2-trifluoroethyl ether (TFETFE) with high thermal stability, superb oxidation tolerance, and a low relative permittivity ($\varepsilon = 6.5$, 298 K) is selected as the NL cosolvent.[12] The ratio of LiFSI/DME and NL cosolvent was fixed to be 1:1. Firstly, the CE profiles of Li plating/stripping on Cu were measured to demonstrate the cycling reversibility of Li metal anode in various electrolytes at a moderate current density of 1.0 mA cm^{-2} and an areal capacity of 1.0 mAh cm^{-2} via the routine method (Method 1, Figure 1a). Compared to the electrolyte without NL cosolvent, the average CE within the initial ten cycles is increased from 97.6% to 98.2% in electrolyte containing NL cosolvent. To further exclude the Li loss associated with the side reaction between Li and Cu as well as the surface roughness of the substrate, the CE was more strictly evaluated under Zhang's method (Method 2).[13] The average CE of repeated Li plating/stripping for 50 cycles is determined to be as high as 99.4% in the NL cosolvent-containing electrolyte, considerably higher than 97.7% in the control electrolyte at 0.5 mA cm^{-2}/1.0 mAh cm^{-2} (Figure 1b).

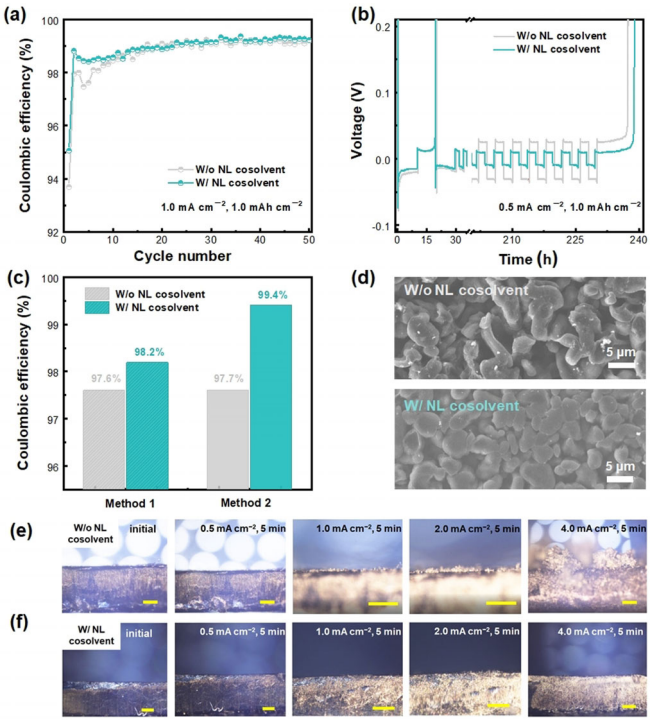

Figure 1. Electrochemical performances and morphology characterizations of Li | Cu cells with and without NL cosolvent. a) Coulombic efficiency of Li | Cu cells measured by method 1 at 1.0 mA cm^{-2} and 1.0 mAh cm^{-2}. b) Long-term voltage-time profile measured by method 2 at 0.5 mA cm^{-2} and 1.0 mAh cm^{-2}. c) The average CE of Li | Cu cells determined via both Method 1 and Method 2. d) SEM images of 1.0 mAh cm^{-2} Li deposits on Cu foils at 0.5 mA cm^{-2}. In-situ optical characterization of Li deposition process in the electrolyte e) without NL cosolvent and f) with the electrolyte containing NL cosolvent. The scale bar is 200 μm.

The discrepancy in CEs determined via both Method 1 and Method 2 was intuitively compared in Figure 1c. Even at higher current densities of 1.0 and 2.0 mA cm^{-2}, enhanced CEs (99.3% and 98.2%, respectively) can be achieved in the electrolyte with NL cosolvent (Figure S1). The elevated CEs are intrinsically associated with the flatter and denser Li plating morphology as recorded in Figure 1d, Figure S2, and Figure 1e,f under scanning electron microscopy and optical microscopy, respectively, which are consistent with the apparently low interfacial resistance measured under electrochemical impedance spectroscopy (EIS) (Figure S3).

The SEI layers play a critical role in the distinct cycling performance of Li metal anodes. X-ray photoelectron spectroscopy (XPS) was performed to track the differences of SEI generated in electrolytes with and without NL cosolvent (Figure 2a, b). As shown in F 1s spectra, SEI formed in the

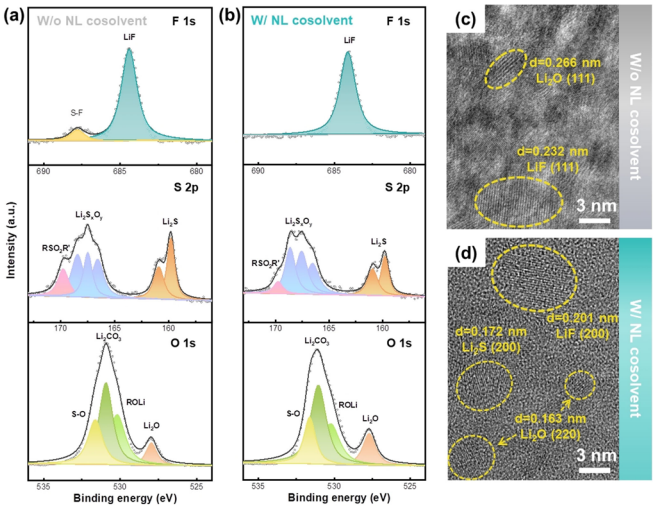

Figure 2. The compositions and structures of SEI in different electrolytes. XPS spectra of SEI formed in the electrolytes a) without and b) with NL cosolvent, respectively. STEM characterizations of SEI formed in electrolytes c) without and d) with NL cosolvent, respectively.

presence of NL cosolvent exhibits a strong Li-F peak (684.8 eV) but negligible S-F (684.8 eV) peak, indicating the more complete decomposition of FSI^- anion. In contrast, a striking S-F peak is observed in the case without NL cosolvent. The incomplete decomposition of FSI^- can further be corroborated by the sharp R-SO_2-R′ peak (169.5 eV) in S 2p spectrum and the weak Li_2O peak (528.2 eV) in O 1s spectrum. The spectra recorded after sputtering further indicates that the SEI formed in the electrolyte with NL cosolvent consisted of more complete decomposition products of FSI^- such as LiF, Li_2S, Li_2O, et al. (Figure S4). Moreover, the contents of F, S elements stemming from anion decomposition both increase (from 3.1% to 3.6%, from 1.8% to 1.9%, respectively), while the atomic fraction of O element originated mainly from solvent reduction products decreases from 28.8% to 26.5% (Figure S5), depicting a stronger anion decomposition tendency on the introduction of NL cosolvent. The XPS results strongly depict that the

reduction of FSI^- anion is facilitated with the presence of NL cosolvent, triggering the generation of an upgraded anion-derived inorganic-rich SEI, which are echoed with the analysis based on scanning transmission electron microscopy (STEM). The crystal lattices captured under STEM indicates that the SEI formed in control electrolyte is composed of less products decomposed from FSI^- (Figure 2c), whereas more abundant LiF, Li_2O, and Li_2S are observed in the SEI generated in NL cosolvent-containing electrolyte (Figure 2d). The substantial inorganic components significantly enhance the mechanical strength of SEI from 3.0 GPa to 8.5 GPa (Figure S6). The enhanced SEI mechanical modulus is believed to play a critical role in suppressing dendrites growth and enhancing the cycling reversibility of working Li metal anodes.

The discrepant SEI characteristics are directly correlated to the distinct Li^+ solvation structure in these two model electrolytes and the preferential decomposition of electrolyte ingredients. Raman spectroscopy was performed to experimentally elucidate the solvation behavior (Figure 3a and Figure S7). With the increasing salt concentration from 1.0 to 3.0 M, the peak of the free FSI^- (717 cm^{-1}) largely reduces (from 74.8% to 27.6%) while the contact ion pairs (CIP, one

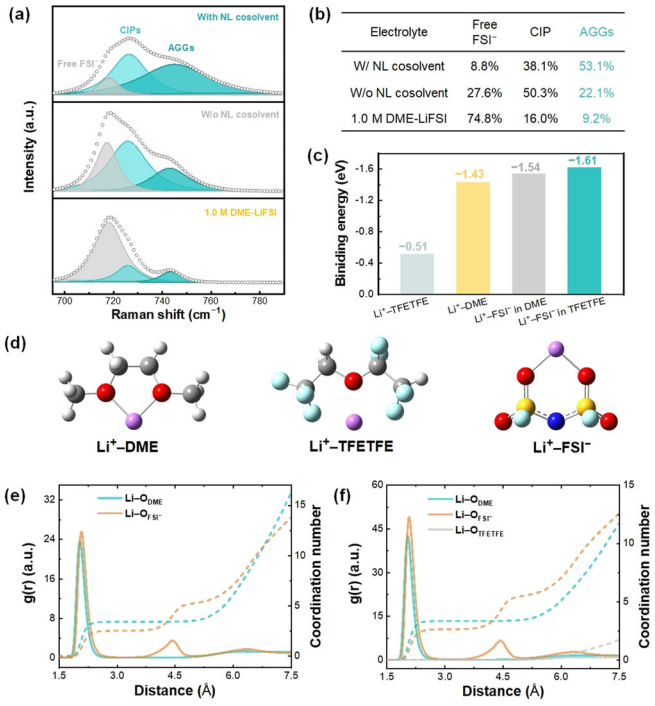

Figure 3. The characterizations of solvation structures. a) Raman spectra of different electrolytes. b) The statistics on the ratio of different coordinates (free anion, CIPs, AGGs) contained in the electrolytes with/without NL cosolvent, which are determined by the corresponding peak areas in Raman spectra. c) The binding energies between Li^+ and various species calculated by DFT. d) The optimized geometrical configurations between Li^+ and solvents/anions. H white, Li purple, C grey, N blue, O red, F light blue, and S yellow. The radial distribution function (solid lines) and coordination number plots (broken lines) of Li-O_{DME}, Li-O_{FSI^-} and Li-O_{TFETFE} pairs calculated from MD simulation trajectories in the electrolytes e) without and f) with NL cosolvent.

FSI^- coordinating to one Li^+, 726 cm^{-1}) becomes the dominant configuration (from 16.0% to 50.3%) (Figure 3a, b). Moreover, the proportion of aggregate clusters (AGGs, one FSI^- coordinating to two or more Li^+, near 743 cm^{-1}) is also enhanced from 9.2% to 22.1%. This is consistent with the current understanding of the salt concentration effects on solvation structure.[8,14] More critically, the anion-cation interaction becomes even stronger after introducing NL cosolvent, where the FSI^- anion exists predominantly as AGGs configuration (53.1%). This strongly indicates the significant influence of NL cosolvent on primary Li^+ solvation structure.

Density functional theory (DFT) calculations and molecular dynamics (MD) simulations were conducted in this work. Firstly, the binding energy between Li^+ and TFETFE cosolvent (−0.51 eV) is essentially weaker than that of other coordinated structures (Figure 3c), indicating that TFETFE is not likely to be recruited into the Li^+ solvation shells. Despite the absence of TFETFE NL cosolvent in primary solvation shell, its low permittivity property strongly alters the electrostatic interaction between Li^+ and FSI^- anion according to classical physiochemical laws.[15] The binding energy between Li^+ and FSI^- is increased from −1.54 to −1.61 eV, illustrating a stronger ion association in the electrolyte containing NL cosolvent. This significantly reduces the reductive stability of FSI^- for more complete decomposition.[16] The corresponding configurations between Li^+ and solvent/anion in DFT calculations are illustrated in Figure 3d. MD simulation was further conducted to investigate the solvation structures in different electrolytes (Figure S8–10). Two sharp peaks corresponding to the Li-O_{DME} and Li-O_{FSI^-} pairs are identified at ≈2.0 Å for both electrolytes, while one small and wide peak of Li-O_{TFETFE} pair at ≈6.3 Å is observed for the electrolyte with NL cosolvent in radial distribution functions, which further confirms the negligible interaction between Li^+ and TFETFE (Figure 3d, e). Critically, after the introduction of NL cosolvent, an apparent trend shows that the coordination number of DME with Li^+ is reduced from 3.4 to 3.3 while the FSI^- anion coordination number enlarges from 2.5 to 2.6, agreeing with the coordinated species distribution statistics obtained from MD simulations (Figure S11). The increased anion coordination number strongly implies that FSI^- anions are more readily participating into inner Li^+ solvation shell (Figure S12). Accordingly, the AGGs with strong ion association dominate the solvation structures in the electrolyte with NL cosolvent.

The altering of coordination structures after the addition of NL cosolvent greatly determines the preferential decomposition of electrolyte at the anode-electrolyte interface. Zeta potential measurement was performed to identify surface charge property of Li metal. As shown in Figure 4a, the data indicates that the lithium surface is negatively charged in both electrolytes of interest. This results from the spontaneous escape of Li ions from Li metal surface into electrolyte, consistent with the previous publication.[17] Therefore, substantial negative surplus charges will accumulate at the electrode surface, which induces cation enrichment within the electric double layer while negatively charged free FSI^- anions are rejected to approach the electrode surface. The

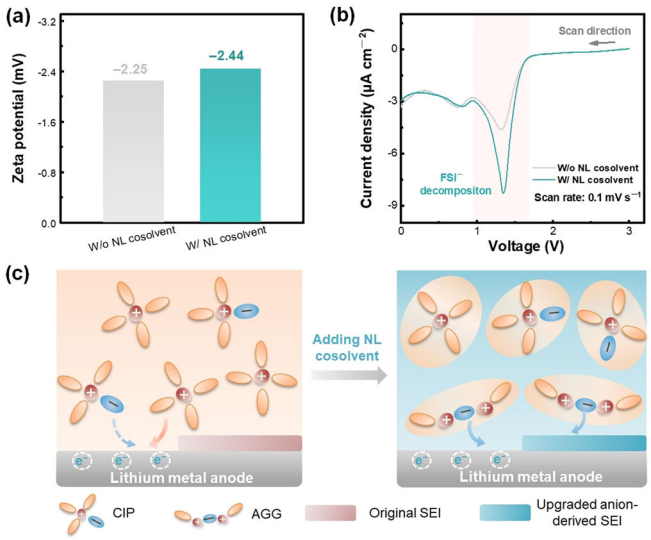

Figure 4. The analysis of preferential electrolyte decomposition behavior. a) Zeta potential measurement of Li metal electrodes in electrolytes with/without NL cosolvent. b) CV profiles of Li | Cu cells at 0.1 mVs^{-1}. c) Schematic illustrations of the working mechanism of NL cosolvent on the solvation structures and thereafter the SEI formation process.

introduction of NL cosolvent largely enhances the ion association and results in AGGs-dominated solvation structures. These associated solvation clusters are positively charged, allowing more FSI^- anion present in an electric double layer, which leads to enhanced decomposition kinetics of FSI^- during SEI construction. As displayed in Figure 4b, a sharp FSI^- decomposition peak is observed in the electrolyte with NL cosolvent, while a relatively weak peak is obtained in the control electrolyte. The enlarged FSI^- anion decomposition peak can also be observed even though the DME base solvent was replaced as other solvents (Figure S13), demonstrating that it is a general behavior that the anion decomposition kinetics can be enhanced with the addition of NL cosolvent. Such a kinetics enhancement of anion decomposition cannot completely be attributed to the decrease of electrolyte viscosity (Figure S14). Besides, no additional peak is observed in CV profiles after the addition of NL cosolvent, suggesting its remarkable thermodynamic stability towards Li metal (Figure 4b).

A schematic illustration is presented in Figure 4c to describe the working scenario of the NL cosolvent strategy. Benefited from the low permittivity and weak binding strength with Li^+ of the NL cosolvent, the inherent interaction between anion and cation can be enhanced, leading to more anion recruitment into the Li^+ solvation sheath to form AGGs. The positively charged associated AGG structure can be locally enriched at Li metal surface and be preferentially reduced with fast kinetics. The as-formed upgraded anion-derived SEI is highly beneficial for reversible Li plating/stripping cycling.

In terms of the above rationale, other NL cosolvent systems were further investigated as confirmation. As an another compatible fluorinated ether with a poor cationic solvation capability (−0.60 eV, Figure S15) and low permittivity ($\varepsilon = 6.2$),[18] 1,1,2,2-tetrafluoroethyl-2,2,3,3-tetrafluoropropyl ether (HFE) was incorporated in our study. Similar to the observations in TFETFE system, the percentage of the strongly associated AGGs largely increases compared to the NL cosolvent-free electrolyte (from 22.1% to 67.6%) under Raman spectroscopy (Figure S16a, b), which enormously enhances the average CE in Li | Cu cell via different methods (Figure S16c, d).

Although fluorinated ether has been adopted as the most common NL cosolvent in literatures, to broaden the scope of this work, more solvents with poor solvation capability and low electricity were introduced to identify the boundary conditions to become a suitable NL cosolvent. The properties of benzene cosolvent-containing electrolyte were investigated. On the one hand, benzene solvent possesses a considerably low dielectric constant of 2.3. On the other hand, the binding energy of benzene toward Li^+ is −0.90 eV (Figure S15), considerably lower than that of DME (−1.43 eV). Consistent with the results of fluorinated ether cosolvents discussed above, the Raman spectroscopy displays a 28.0% increase in the ratio of AGG structure after the addition of benzene cosolvent (Figure 5a, b). Accordingly, Li | Cu half cell demonstrates an extremely high average CE of 99.6% (Figure 5c). The results unambiguously indicate that benzene with both a low permittivity and poor solvation capability can serve as an admirable cosolvent and largely enhance the lithium utilization. In contrast, the introduction of a novel cosolvent 1,4-dioxane (1,4-DX) with similarly low dielectric constant ($\varepsilon = 2.2$) but relatively stronger binding strength towards Li^+ (−1.13 eV) largely increases the ratio of free FSI^- compared to original 3.0 M LiFSI/DME electrolyte (from 27.6% to 56.1%, Figure 5a, b). As a result, the average CE of 1,4-DX cosolvent electrolyte was determined to be 97.6% (Figure 5d), even lower than that with original electrolyte. The difference in CE can also be observed in Li | Cu cells with

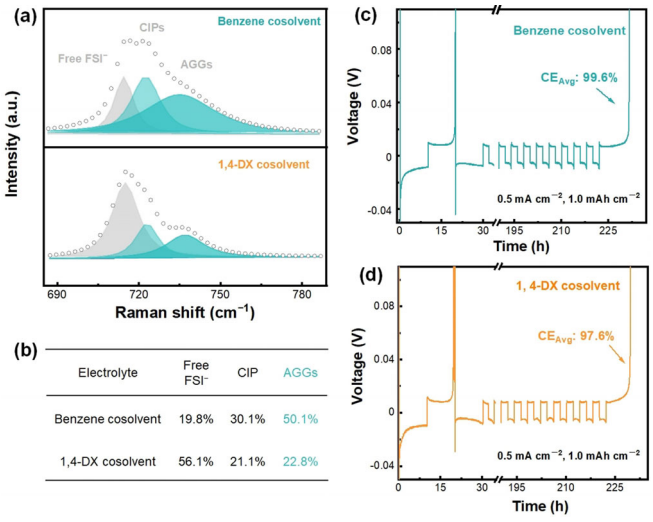

Figure 5. The solvation structures and cycling performance of electrolytes with other two cosolvents. a) Raman spectra and b) the statistics on the ratio of different coordinates in the electrolytes with benzene or 1,4-DX cosolvent. c),d) Cycling performance of Li | Cu cells at 0.5 mAcm^{-2} and 1.0 mAhcm^{-2} using benzene cosolvent and 1,4-DX cosolvent electrolytes, respectively.

traditional evaluation methodology (Figure S17). The reduced reversibility of Li plating/stripping can be attributed to the inferior SEI with less anion participation.

It is also noteworthy that although the dielectric property and solvation capability of the cosolvent are critically valued in this work, other properties such as the compatibility toward Li metal are also important factors to be considered. To understand this issue, dimethyl carbonate (DMC) cosolvent with a low dielectricity but extreme instability toward Li metal was introduced as a comparison (Figure S18).[19] Despite the similar Li^+ solvation structure distribution with 1,4-DX cosolvent-containing electrolytes (Figure 5a, b), the performance of Li | Cu cell containing DMC cosolvent is much worse. The half cell quickly failed within only three plating/stripping cycles, which reflects the extremely unstable SEI in the presence of DMC cosolvent. Hence, NL cosolvent simultaneously possessing considerable thermodynamic compatibility toward Li metal should be exploited to power future stable Li metal batteries.

To further elucidate the boundary conditions of suitable NL cosolvents, a solvent diagram with regard to binding energy towards Li^+ and dielectric constant was elaborately concluded (Figure 6). A descriptor of relative binding energy ($E_{DME}-E_{solvent}$) was adopted to predict the actual solvation tendency of the cosolvents compared to base solvent DME. A large relative binding energy value indicates the inferior solvation capability of the corresponding cosolvent, which contributes to the preservation of the original cation-anion CIPs and AGGs. In addition to the weak interaction towards Li cations, lower permittivity compared to base solvent is another prerequisite for an ideal NL cosolvent. The low dielectric environment afforded by cosolvent can effectively enhance the inherent interaction between anion and cation, leading to more anion recruitment into the Li^+ solvation sheath to form AGGs and therefore facilitate anion decomposition. According to such paradigm, the superior cycle performance of Li metal anodes after the introduction of cosolvent which have both non-solvating and low-dielectricity characteristics such as nonpolar alkanes (hexane, etc),[20] fluorinated ether (bis(2,2,2-trifluoroethyl) ether [BTFE],[21] TFETFE, HFE, etc), aromatic compound (Benzene, etc) can be accurately comprehended. In brief, the solvent diagram which predicts suitable NL cosolvent not only coincides the experimental results in our and previous works,[20–22] but also provides effective guidance to rationally optimize the cosolvents for stable Li metal batteries.

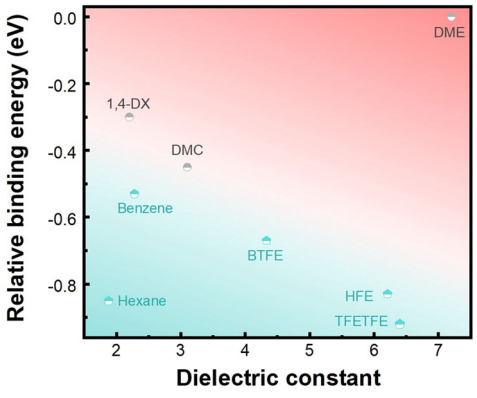

Figure 6. The solvent diagram with regard to relative binding energy towards Li^+ and dielectric constant. The cosolvents with lower permittivity and larger relative binding energy (cyan region) compared to base solvent (DME herein) effectively enhance the binding strength of Li^+ cation with anion and thus accelerate the generation of aggregate clusters, which favors the complete decomposition of anion to form an upgraded anion-derived inorganic-rich SEI.

Conclusion

The introduction of NL cosolvent can significantly enhance the binding strength of Li^+ cation with anion and regulate the solvation structures in electrolytes. The AGG coordination structures dominate in bulk electrolyte benefited from the low-permittivity environment afforded by the NL cosolvent, favoring more FSI^- anions accumulation at the negatively charged Li surface. The enriched anions are thereafter preferentially reduced to generate an upgraded anion-derived inorganic-rich SEI. Furthermore, a solvent diagram is concluded in terms of the descriptors of relative binding energy towards Li^+ and dielectric constant to explicitly illuminate the prerequisites of a promising NL cosolvent. This work elucidates the critical importance of fundamental physiochemical principle in electrolyte design, indicative for a new outlet to explore novel non-solvating, low-dielectricity, and highly compatible cosolvents for next-generation Li metal batteries.

Acknowledgements

This work was supported by the Beijing Natural Science Foundation (JQ20004, L182021), National Key Research and Development Program (2016YFA0202500), the National Natural Science Foundation of China (21776019), and Scientific and Technological Key Project of Shanxi Province (20191102003).

Conflict of interest

The authors declare no conflict of interest.

Keywords: anion–cation interaction · cation solvation · lithium metal batteries · low-dielectricity cosolvent · solid electrolyte interphase

[1] W. Xu, J. Wang, F. Ding, X. Chen, E. Nasybutin, Y. Zhang, J.-G. Zhang, *Energy Environ. Sci.* **2014**, *7*, 513–537; C. Yan, R. Xu, Y. Xiao, J.-F. Ding, L. Xu, B.-Q. Li, J.-Q. Huang, *Adv. Funct. Mater.* **2020**, 1909887; Y. R. Liang, Y. Xiao, C. Yan, R. Xu, J. F. Ding, J. Liang, H. J. Peng, H. Yuan, J. Q. Huang, *J. Energy Chem.* **2020**, *48*, 203–207; J. B. Goodenough, Y. Kim, *Chem. Mater.* **2010**, *22*, 587–603.

[2] C. Yan, H. Yuan, H. S. Park, J. Q. Huang, *J. Energy Chem.* **2020**, *47*, 217–220.

[3] C. Fang, X. Wang, Y. S. Meng, *Trends Chem.* **2019**, *1*, 152 – 158; Y. Zhu, V. Pande, L. Li, B. Wen, M. S. Pan, D. Wang, Z. F. Ma, V. Viswanathan, Y. M. Chiang, *Proc. Natl. Acad. Sci. USA* **2020**, *117*, 27195 – 27203; N. D. Trinh, D. Lepage, D. Aymé-Perrot, A. Badia, M. Dollé, D. Rochefort, *Angew. Chem. Int. Ed.* **2018**, *57*, 5072 – 5075; *Angew. Chem.* **2018**, *130*, 5166 – 5169; R. Xu, C. Yan, Y. Xiao, M. Zhao, H. Yuan, J.-Q. Huang, *Energy Storage Mater.* **2020**, *28*, 401 – 406.

[4] J. Zheng, M. S. Kim, Z. Tu, S. Choudhury, T. Tang, L. A. Archer, *Chem. Soc. Rev.* **2020**, *49*, 2701 – 2750; K. Yan, J. Wang, S. Zhao, D. Zhou, B. Sun, Y. Cui, G. Wang, *Angew. Chem. Int. Ed.* **2019**, *58*, 11364 – 11368; *Angew. Chem.* **2019**, *131*, 11486 – 11490; A. B. Gunnarsdottir, C. V. Amanchukwu, S. Menkin, C. P. Grey, *J. Am. Chem. Soc.* **2020**, *142*, 20814 – 20827; Z. Wang, F. Qi, L. Yin, Y. Shi, C. Sun, B. An, H. M. Cheng, F. Li, *Adv. Energy Mater.* **2020**, *10*, 1903843.

[5] J.-F. Ding, R. Xu, C. Yan, B.-Q. Li, H. Yuan, J.-Q. Huang, *J. Energy Chem.* **2021**, *59*, 306 – 319; A. Kushima, K. P. So, C. Su, P. Bai, N. Kuriyama, T. Maebashi, Y. Fujiwara, M. Z. Bazant, J. Li, *Nano Energy* **2017**, *32*, 271 – 279; W. Liu, P. Liu, D. Mitlin, *Adv. Energy Mater.* **2020**, *10*, 2002297.

[6] J. Zhao, L. Liao, F. Shi, T. Lei, G. Chen, A. Pei, J. Sun, K. Yan, G. Zhou, J. Xie, C. Liu, Y. Li, Z. Liang, Z. Bao, Y. Cui, *J. Am. Chem. Soc.* **2017**, *139*, 11550 – 11558; J. F. Ding, R. Xu, C. Yan, Y. Xiao, L. Xu, H. J. Peng, H. S. Park, J. Liang, J. Q. Huang, *Nano Select* **2020**, *1*, 94 – 110; R. Xu, C. Yan, J.-Q. Huang, *Trends Chem.* **2020**, *3*, 5 – 14; Z.-J. Zheng, Q. Su, Q. Zhang, X.-C. Hu, Y.-X. Yin, R. Wen, H. Ye, Z.-B. Wang, Y.-G. Guo, *Nano Energy* **2019**, *64*, 103910.

[7] S. Chen, J. Zheng, D. Mei, K. S. Han, M. H. Engelhard, W. Zhao, W. Xu, J. Liu, J.-G. Zhang, *Adv. Mater.* **2018**, *30*, 1706102; X. Fan, X. Ji, L. Chen, J. Chen, T. Deng, F. Han, J. Yue, N. Piao, R. Wang, X. Zhou, X. Xiao, L. Chen, C. Wang, *Nat. Energy* **2019**, *4*, 882 – 890; X. Chen, Q. Zhang, *Acc. Chem. Res.* **2020**, *53*, 1992 – 2002; Y. Xu, H. Wu, Y. He, Q. Chen, J. G. Zhang, W. Xu, C. Wang, *Nano Lett.* **2020**, *20*, 418 – 425.

[8] N. Piao, X. Ji, H. Xu, X. Fan, L. Chen, S. Liu, M. N. Garaga, S. G. Greenbaum, L. Wang, C. Wang, X. He, *Adv. Energy Mater.* **2020**, *10*, 1903568.

[9] W. Zhang, Z. Shen, S. Li, L. Fan, X. Wang, F. Chen, X. Zang, T. Wu, F. Ma, Y. Lu, *Adv. Funct. Mater.* **2020**, *30*, 2003800.

[10] J. Wang, Y. Yamada, K. Sodeyama, C. H. Chiang, Y. Tateyama, A. Yamada, *Nat. Chem.* **2016**, *7*, 12032.

[11] X. Ren, L. Zou, X. Cao, M. H. Engelhard, W. Liu, S. D. Burton, H. Lee, C. Niu, B. E. Matthews, Z. Zhu, C. Wang, B. W. Arey, J. Xiao, J. Liu, J.-G. Zhang, W. Xu, *Joule* **2019**, *3*, 1662 – 1676; J. Chen, X. Fan, Q. Li, H. Yang, M. R. Khoshi, Y. Xu, S. Hwang, L. Chen, X. Ji, C. Yang, H. He, C. Wang, E. Garfunkel, D. Su, O. Borodin, C. Wang, *Nat. Energy* **2020**, *5*, 386 – 397; C. Yan, Y. X. Yao, W. L. Cai, L. Xu, S. Kaskel, H. S. Park, J. Q. Huang, *J. Energy Chem.* **2020**, *49*, 335 – 338.

[12] C. Wohlfarth, Static Dielectric Constants of Pure Liquids and Binary Liquid Mixtures, **2008**.

[13] B. D. Adams, J. Zheng, X. Ren, W. Xu, J.-G. Zhang, *Adv. Energy Mater.* **2017**, *8*, 1702097.

[14] X. Ren, S. Chen, H. Lee, D. Mei, M. H. Engelhard, S. D. Burton, W. Zhao, J. Zheng, Q. Li, M. S. Ding, M. Schroeder, J. Alvarado, K. Xu, Y. S. Meng, J. Liu, J.-G. Zhang, W. Xu, *Chem* **2018**, *4*, 1877 – 1892.

[15] X. Chen, X.-Q. Zhang, H.-R. Li, Q. Zhang, *Batteries Supercaps* **2019**, *2*, 128 – 131.

[16] W. Shin, L. Zhu, H. Jiang, W. F. Stickle, C. Fang, C. Liu, J. Lu, X. Ji, *Mater. Today* **2020**, *40*, 63 – 71; X. Chen, H. R. Li, X. Shen, Q. Zhang, *Angew. Chem. Int. Ed.* **2018**, *57*, 16643 – 16647; *Angew. Chem.* **2018**, *130*, 16885 – 16889.

[17] R. Xu, X. Shen, X. X. Ma, C. Yan, X. Q. Zhang, X. Chen, J. F. Ding, J. Q. Huang, *Angew. Chem. Int. Ed.* **2021**, *60*, 4215 – 4220; *Angew. Chem.* **2021**, *133*, 4261 – 4266; S. Honary, F. Zahir, *J. Pharm. Res.* **2013**, *12*, 255.

[18] K. Dokko, N. Tachikawa, K. Yamauchi, M. Tsuchiya, A. Yamazaki, E. Takashima, J.-W. Park, K. Ueno, S. Seki, N. Serizawa, M. Watanabe, *J. Electrochem. Soc.* **2013**, *160*, A1304 – A1310.

[19] S.-K. Jeong, M. Inaba, Y. Iriyama, T. Abe, Z. Ogumi, *Electrochim. Acta* **2002**, *47*, 1975 – 1982; C. Fang, J. Li, M. Zhang, Y. Zhang, F. Yang, J. Z. Lee, M.-H. Lee, J. Alvarado, M. A. Schroeder, Y. Yang, B. Lu, N. Williams, M. Ceja, L. Yang, M. Cai, J. Gu, K. Xu, X. Wang, Y. S. Meng, *Nature* **2019**, *572*, 511 – 515.

[20] C. V. Amanchukwu, X. Kong, J. Qin, Y. Cui, Z. Bao, *Adv. Energy Mater.* **2019**, *9*, 1902116.

[21] S. Chen, J. Zheng, L. Yu, X. Ren, M. H. Engelhard, C. Niu, H. Lee, W. Xu, J. Xiao, J. Liu, J.-G. Zhang, *Joule* **2018**, *2*, 1548 – 1558; M. L. Gordin, F. Dai, S. Chen, T. Xu, J. Song, D. Tang, N. Azimi, Z. Zhang, D. Wang, *ACS Appl. Mater. Interfaces* **2014**, *6*, 8006 – 8010.

[22] L. Xiao, Z. Zeng, X. Liu, Y. Fang, X. Jiang, Y. Shao, L. Zhuang, X. Ai, H. Yang, Y. Cao, J. Liu, *ACS Energy Lett.* **2019**, *4*, 483 – 488; D. J. Yoo, S. Yang, K. J. Kim, J. W. Choi, *Angew. Chem. Int. Ed.* **2020**, *59*, 14869 – 14876; *Angew. Chem.* **2020**, *132*, 14979 – 14986.

Manuscript received: February 2, 2021
Accepted manuscript online: March 2, 2021
Version of record online: ■■ ■■, ■■■■

Research Articles

Lithium Metal Batteries

J.-F. Ding, R. Xu, N. Yao, X. Chen, Y. Xiao, Y.-X. Yao, C. Yan, J. Xie, J.-Q. Huang* ———— ▮▮▮▮–▮▮▮▮

Non-Solvating and Low-Dielectricity Cosolvent for Anion-Derived Solid Electrolyte Interphases in Lithium Metal Batteries

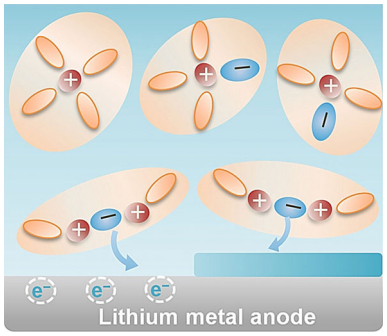

The introduction of cosolvents with non-solvating and low-dielectricity (NL) properties can intrinsically enhance the interaction between anion and Li^+ and regulate the solvation structures in electrolytes, which favors an upgraded anion-derived solid electrolyte interphase (SEI) on lithium metal anodes.